M. J. COLEMAN

**Department of Mechanical and
Aerospace Engineering
Cornell University, Ithaca, NY 14853-7501 U.S.A
coleman@tam.cornell.edu**

P. HOLMES

**Department of Mechanical and
Aerospace Engineering, Princeton University, Princeton, NJ
08544-5263 U.S.A
Program in Applied and Computational Mathematics
Princeton University, Princeton, NJ 08544-1000, U.S.A
E-mail: pholmes@Princeton.EDU**

MOTIONS AND STABILITY OF A PIECEWISE HOLONOMIC SYSTEM: THE DISCRETE CHAPLYGIN SLEIGH

Received June 23, 1999

We discuss the dynamics of a piecewise holonomic mechanical system: a discrete sister to the classical nonholonomically constrained Chaplygin sleigh. A slotted rigid body moves in the plane subject to a sequence of pegs intermittently placed and sliding freely along the slot; motions are smooth and holonomic except at instants of peg insertion. We derive a return map and analyze stability of constant-speed straight-line motions: they are asymptotically stable if the mass center is in front of the center of the slot, and unstable if it lies behind the slot; if it lies between center and rear of the slot, stability depends subtly on slot length and radius of gyration. As slot length vanishes, the system inherits the eigenvalues of the Chaplygin sleigh while remaining piecewise holonomic. We compare the dynamics of both systems, and observe that the discrete skate exhibits a richer range of behaviors, including coexistence of stable forward and backward motions.

1. Introduction

Although conservative nonholonomic systems lack dissipation, their constraints can permit these systems to enjoy asymptotically stable steady motions in certain cases. In particular, kinematic couplings due to nonholonomic constraints arise that can stabilize steady motions. A well-known example, and the subject of this paper, is the Chaplygin sleigh (or skate), in which the constraint couples heading angle rate and velocity, allowing exponentially stable motions in the plane.

A related class of *piecewise holonomic* mechanical systems with intermittent contacts that are smooth and holonomic everywhere except at instants of transition are briefly discussed in Ruina [17]. Examples of such devices are the uncontrolled, unpowered walking machines pioneered by Tad McGeer [11, 12, 13, 7, 6] which exhibit smooth inverted pendulum-like motions interrupted by dissipative joint and foot collisions with the ground as they walk stably and somewhat human-like down shallow slopes. The model described in this paper was moreover a motivating example for the planar legged insect locomotion models of Schmitt and Holmes [19]. Piecewise holonomic systems such as these passive-dynamic walkers can be thought of as nonholonomically constrained in their overall motion in the following sense: the dimension of the configuration space is greater than the instantaneous dimension of the velocity space [17]. Such nonconservative, piecewise holonomic systems can also exhibit asymptotically stable behavior.

Mathematics Subject Classification

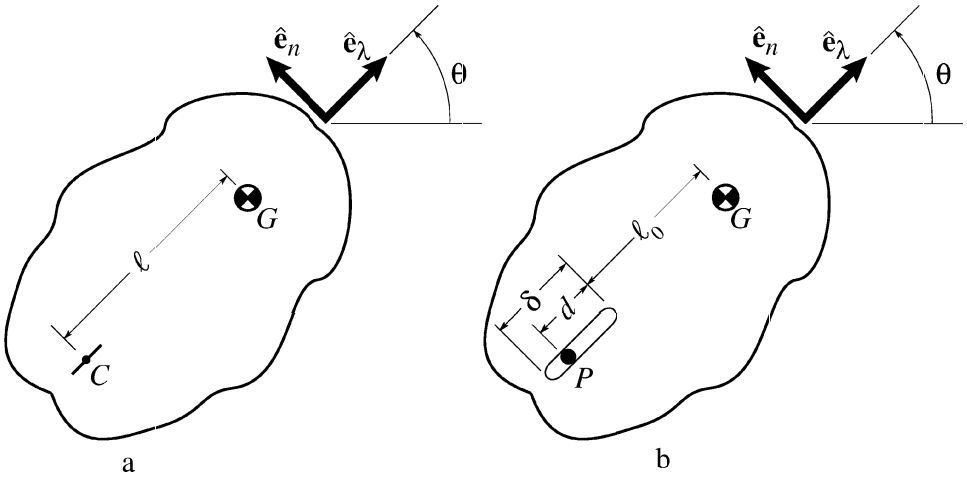

Fig. 1. a) The Chaplygin sleigh and b) the sleigh's discrete holonomic sister system. A sequence of pegs fixed to the plane slide frictionlessly in the slot at P. (Schematic from Ruina [17].)

The question of whether the stability of such systems is due solely to dissipation, solely to nonholonomy, or to both was examined in Ruina [17] by studying a simple 2D example of a smooth (conservative) nonholonomic system, the Chaplygin sleigh (Neimark and Fufaev [14]), and comparing it to a discrete (dissipative) sister system in the limit as dissipation tends to zero while its piecewise holonomic nature is maintained. The governing equations of the discrete system were found to reduce to those of the smooth system, to first order in a characteristic length; thus, since the eigenvalues for the smooth skate indicate exponential stability, those of the discrete system must do likewise. Eigenvalues for the discrete system were not however calculated by Ruina [17], so direct stability comparisons could not be made.

In Sections 3–4 of this paper we further study the discrete skate, comparing its behavior to that of the smooth Chaplygin sleigh, the governing equations of which are reviewed in Section 2. In the limit as the characteristic length goes to zero, the discrete system remains piecewise holonomic while dissipation tends to zero; thus, asymptotic stability of the discrete system cannot be due to dissipation, and depends only on the nonholonomic nature of its discrete holonomy [17]. (The elastic-legged models of [19] are likewise discretely holonomic; although these models are controlled, the energy of control may be made arbitrarily small.) The dynamics of the discrete skate is remarkably rich, and we believe that this explicitly soluble example will further the analysis and understanding of more complex piecewise holonomic problems.

2. The Chaplygin Sleigh: Smooth Skate Model

We summarize the analysis of the Chaplygin sleigh (see Figure 1(a)). A body has mass m with center of mass G about which its polar moment of inertia is I. At point C, a distance ℓ from G, a frictionless skate constrains the direction of motion, so that the velocity of C is $\mathbf{v}_C = v\hat{\mathbf{e}}_\lambda$ and the force acting on the body at C is $F\hat{\mathbf{e}}_n$. Velocity may be positive or negative; i. e., the skate can reverse direction. The angle θ specifies orientation in the inertial plane. Including rotation, the absolute velocity of the mass center G is $\mathbf{v}_G = v\hat{\mathbf{e}}_\lambda + \ell\dot{\theta}\hat{\mathbf{e}}_n$.

The sleigh is nonholonomic in the following sense: three coordinates are needed to specify orientation and position on the plane, yet its velocity space is defined by only two variables, velocity of the contact point along the skate direction and angular speed. Although its configuration space is three dimensional, the skate has only two degrees of freedom at any instant.

2.1. Governing Equations, Steady Solutions, and Stability

We derive the governing equations via linear and angular momentum balance. Subsequently, we will discuss its behavior in terms of energy and angular momentum in order to make comparisons to the discrete skate. But, to calculate the angular momentum of the skate as a function of arc length with respect to a point on the ground coincident at each instant with a point on the skate blade, we must solve its differential equations of motion. In addition, to find where on its path the skate may change direction, we will need the velocity of point C as function of position.

Linear momentum balance and angular momentum balance about C', the non-accelerating point in an inertial reference frame instantaneously coincident with point C on the sleigh, yield the following system of nondimensionalized equations governing the evolution of V, the speed of point C, and $\Omega = \dot{\theta}$, the angular rate of the body:

$$\dot{S} = V\,, \qquad \dot{V} = L\Omega^2\,, \qquad \dot{\theta} = \Omega\,, \qquad \dot{\Omega} = -\frac{L}{L^2+1}\,V\Omega\,, \tag{2.1}$$

where

$$L = \frac{\ell}{\rho}\,, \quad S = \frac{s}{\rho}\,, \quad V = \frac{v}{v_0}\,, \quad \Omega = \frac{\omega}{v_0}\rho\,, \quad \omega = \frac{d\theta}{dt}\,, \quad (\dot{}) = \frac{d(\quad)}{d\tau}\,, \quad \tau = \frac{tv_0}{\rho}\,, \tag{2.2}$$

and v_0 is the initial speed of point C. The nondimensional arc length, S, along the path of the skate contact point C is taken to be positive for forward *and* backward motions. Length measures have been scaled with respect to the radius of gyration

$$\rho \equiv \sqrt{\frac{I}{m}}\,. \tag{2.3}$$

The nondimensionalization in Equation (2.2) prompts the following observation. *The smooth and discrete skates belong to a class of particle and rigid body systems that may interact with any combination of holonomic or nonholonomic constraints, friction (possibly anisotropic) proportional to normal force, collisions with output velocity homogeneous of degree one in input velocity, and drag forces proportional to velocity squared* but without *other forces acting on them (such as those due to gravity, springs, pre-stresses, linear viscosity). Such systems are special in that they enjoy velocity scaling; e. g., double the velocity as a function of position and the resulting solution is still legitimate* [18].

From the viewpoint of non-canonical Hamiltonian systems, the Chaplygin sleigh can be seen as a special case of a generalised Toda lattice [2].

The state vector is $\mathbf{q} = \{S, V, \theta, \Omega\}^T$. There is a two-parameter family of steady solutions: $\mathbf{q}^* = \{V^*\tau, V^*, \theta^*, 0\}^T$, corresponding to straight-line motions. In energy-momentum space, these are

$$H^*_{/C} = (1+L^2)\,\Omega^2 = 0 \quad \text{and} \quad \mathrm{E}^* = \frac{1}{2}(\mathrm{V}^*)^2\,. \tag{2.4}$$

Linearizing the governing equations at $\mathbf{q}^*$ yields the eigenvalues $\xi_{1-3} = 0$ and $\xi_4 = -\dfrac{LV^*}{1+L^2}$. The first three correspond to a family of solutions parameterized by the velocity V^* and heading θ^*; ξ_4 indicates asymptotic stability for $L > 0$. However, for $L < 0$, the skate is unstable. Stability depends on whether the mass center lies in front of or behind the contact point, and its degree, on how far in either direction.

Equations (2.1) can be solved in closed form for V, θ, and Ω as functions of arc length S and their initial values (see Appendix A). Trajectories for arbitrary initial conditions in energy–momentum–arc length phase space are curves with angular momentum exponentially growing ($L < 0$) or decaying ($L > 0$) as functions of arc length, and lying in constant energy planes (see, for example, Figure 4 below).

3. The Discrete Skate Model

Following Ruina [17], we define a piecewise-holonomic sister system to the smooth skate: Figure 1(b). The slotted body slides frictionlessly over a sequence of pegs inserted in and retracted from the plane. Motion begins with a peg at one end of the slot, which slides along the peg until it reaches the other end, when an "external agent" instantaneously retracts it without collision and inserts a new pin at the the starting end, where a collision with the slot's side may occur. If velocity changes sign between collisions, the peg is retracted when it returns to the starting end and the new peg is instead inserted at the other end. This insertion/retraction protocol is identical for forward and for backward motions.

Two mechanical realizations for the external agency are proposed in Ruina [17]:

1. A frictionless chain on a loop on the body has bumps on its bottom at regular intervals; one bump touches the ground at a time acting as a no-bounce, no-slip contact point without torsional resistance. The rest of the mechanism is supported by frictionless contacts. At the instant one bump leaves the plane, another drops down.

2. A massless, rigid, rimless wheel of large radius is attached to a body-fixed horizontal axle. A supporting structure attached to the axle and making frictionless contact with the ground keeps the wheel perpendicular to the plane. The rigid spokes make no-bounce, no-slip collisions without torsional resistance thus acting as a sequence of "ball-and-socket joints." The large radius simplifies the mechanism by decoupling vertical from in-plane dynamics, but is not essential.

Such self-contained devices for peg retraction/insertion permit the discrete skate to be entirely passively stable, in appropriate parameter ranges, without requiring active control over peg placement.

As for the smooth skate, the mass center velocity is $\mathbf{v}_G = v\hat{\mathbf{e}}_\lambda + \ell\dot{\theta}\hat{\mathbf{e}}_n$, the peg/body force is $F\hat{\mathbf{e}}_n$, and orientation is given by the rotation angle θ. The slot of length δ aligned with $\hat{\mathbf{e}}_\lambda$ slides without friction, guided by a peg fixed at point ${}^iP$. Each time a new peg appears at the front of the slot nearer to G, a new point ${}^{i+1}P$ is associated with that location, leaving a trail of points on the plane as the body progresses. The velocity v along the slot, may again be positive or negative.

The distance between G and the front of the slot is ℓ_0, which may be negative; i. e., the mass center may lie before, within or behind the slot. The distance from the peg to the front of the slot is $d(t)$ and the peg's distance to point G is $\ell(t) = \ell_0 + d(t)$. For forward motions, sliding starts when $\ell(t) = \ell_0$. When the peg reaches the end of the slot, $\ell = \ell_0 + \delta$, it loses contact without an impulse, and the newly-inserted peg may make a collision at the front of the slot. If the skate reverses direction between collisions, the peg starts and ends at $\ell(t) = \ell_0$. Thereafter, the skate goes backwards and the peg starts at $\ell(t) = \ell_0 + \delta$ and finishes at $\ell(t) = \ell_0$, and so on. In general, the skate can change direction any number of times.

This system is piecewise holonomic between peg insertion/retractions; the dimensions of configuration space ($d(t)$, $\theta(t)$) and of velocity space ($v(t)$, $\dot{\theta}(t)$) are both two. It can however be viewed as nonholonomically constrained in overall motion: four coordinates are required to specify its position in the plane at any instant ($d(t)$ and $\theta(t)$ *plus* peg position), while the dimension of the velocity space remains two.

As for the smooth skate, we derive governing equations via linear and angular momentum balance. We do this primarily to find where along its path the skate may change direction. Then, since energy and angular momentum are conserved between peg collisions, it is more natural and convenient to write the return map that describes the dynamics in terms of those quantities. The equations for evolution of V, the velocity of the skate along the slot, and Ω, the angular rate of the body, between collisions, may be written in nondimensional form as:

$$\dot{D} = V\,, \qquad \dot{V} = (L_0 + D)\Omega^2\,, \qquad \dot{\theta} = \Omega\,, \qquad \dot{\Omega} = -\frac{2(L_0 + D)}{1 + (L_0 + D)^2} V\Omega\,, \tag{3.1}$$

where we have nondimensionalized as for the smooth skate, with $\rho = \sqrt{\frac{I}{m}}$:

$$L_0 = \frac{\ell_0}{\rho}\,, \quad D = \frac{d}{\rho}\,, \quad V = \frac{v}{v_0}\,, \quad \Omega = \frac{\omega}{v_0}\rho\,, \quad \omega = \frac{d\theta}{dt}\,, \quad \tau = \frac{tv_0}{\rho}\,, \quad \text{and} \quad (\dot{}) = \frac{d(\quad)}{d\tau}\,. \tag{3.2}$$

We also define a nondimensional slot length, $\Delta = \frac{\delta}{\rho}$. The state vector is $\mathbf{q} = \{D, V, \theta, \Omega\}^T$. Equations (3.1) hold between each peg insertion and removal; they may be integrated in closed form: see Appendix B.1 for details. Moreover, as for the smooth skate, angular momentum about the peg and energy are conserved between collisions:

$$E(D) = \frac{1}{2}\left[V^2 + \left(1 + (L_0 + D)^2\right)\Omega^2\right] = E_0 = \text{const}\,, \tag{3.3}$$

$$H_{/P}(D) = \left[1 + (L_0 + D)^2\right]\Omega = H^0_{/P} = \text{const}\,. \tag{3.4}$$

3.1. Poincaré Map, Fixed Points and Stability

To study the behavior of this discrete system, we use a Poincaré section Σ. We sample the phase space at collisions when the distance of the peg along the slot is $d = 0$ for forward motions and $d = \delta$ for backward motion, and define a map $\mathbf{f}$ on Σ that takes the system's state just after a collision to just after the next.

This approach has also been used in other work involving the dynamics of systems with discontinuous vector fields, including: hopping robots (Bühler and Koditschek, 1990 [3]); bouncing balls (Guckenheimer and Holmes, 1983 [8]); elasto-plastic oscillators (Pratap, *et. al.*, 1992 [15, 16]); impact oscillators (Shaw and Holmes, 1983 [20], Shaw and Rand, 1989 [21]); balance wheels and pendula in clocks (Andronov, *et al.* [1]); and walking (McGeer, 1991 [13], Hurmuzlu, 1993 [10, 9], Coleman and Ruina, 1998 [5, 6], Garcia, *et al.*, 1998 [7]).

The Poincaré return map takes the form:

$$^{i+1}\mathbf{q}^+ = \mathbf{f}(^i\mathbf{q}^+) \quad \text{or} \quad {}^i\mathbf{q}^+ \overbrace{\xrightarrow{\mathbf{p}} {}^{i+1}\mathbf{q}^- \xrightarrow{\mathbf{h}}}^{\mathbf{f}} {}^{i+1}\mathbf{q}^+. \tag{3.5}$$

Here the pre-superscript i denotes collision number, and instants directly before and after collision i are denoted by post-superscripts $(-)$ and $(+)$; thus $^i\mathbf{q}^+$ denotes the state following collision i. $\mathbf{f}$ is a composition of two maps: $\mathbf{f} = \mathbf{h} \circ \mathbf{p}$, where $\mathbf{p}$, obtained by integrating the equations of motion (3.1), describes the motion following collision i to just before collision $i + 1$, and $\mathbf{h}$ governs the jump in the state vector incurred at collision $i + 1$.

To compute $\mathbf{f}$, we must therefore augment solutions of (3.1) by a collision rule. Since there are no forces along the slot, the collision impulse acts only in the $\hat{\mathbf{e}}_n$ direction at the new point P. Let ^iP denote the pre-collision peg location and ^{i+1}P the post-collision peg location. Then, neglecting any non-impulsive reactions, angular momentum is conserved about ^{i+1}P, yielding the following nondimensionalized jump conditions for peg position, velocity along the slot, angle, and angular rate (depending on whether velocity prior to collision is positive or negative):

$$\begin{aligned}
^{i+1}D^+ &= \Delta - {}^{i+1}D^-\,,\\
^{i+1}V^+ &= {}^{i+1}V^-\,,\\
^{i+1}\theta^+ &= {}^{i+1}\theta^-\,,\\
^{i+1}\Omega^+ &= \frac{1 + L_0(L_0 + \Delta)}{1 + (L_0 + (\Delta - {}^{i+1}D^-))^2}\,{}^{i+1}\Omega^-\,,
\end{aligned} \tag{3.6}$$

where ${}^{i+1}D^- = \Delta$ for ${}^{i+1}V^- > 0$ and ${}^{i+1}D^- = 0$ for ${}^{i+1}V^- < 0$. In terms of energy and angular momentum, the collision rule implies:

$$\begin{aligned}
{}^{i+1}D^+ &= \Delta - {}^{i+1}D^- \,, \\
{}^{i+1}E^+ &= {}^{i+1}E^- - \frac{1}{2}\frac{\Delta^2}{\left[1+(L_0+{}^{i+1}D^-)^2\right]^2\left[1+(L_0+(\Delta-{}^{i+1}D^-)^2\right]}\left({}^{i+1}H^-_{/P}\right)^2 \,, \\
{}^{i+1}\theta^+ &= {}^{i+1}\theta^- \,, \\
{}^{i+1}H^+_{/P} &= \frac{1+L_0(L_0+\Delta)}{1+(L_0+{}^{i+1}D^-)^2}\,{}^{i+1}H^-_{/P} \,,
\end{aligned} \tag{3.7}$$

with state vector $\mathbf{q} = \{D, E, \theta, H_{/P}\}^T$. Energy and angular momentum conservation between collisions are stated as, respectively, ${}^{i+1}E^- = {}^{i}E^+$ and ${}^{i+1}H^-_P = {}^{i}H^+_P$. Composing (3.7) with explicit solutions of (3.1) given in Appendix B.1 (B.1–B.2), we obtain the return map, which is given in (B.3) and (B.4) of Appendix B.2 for cases in which velocity reversals respectively *do not* and *do* occur between collisions.

3.1.1. Periodic Motions

For periodic motions of the discrete skate, we must find n-periodic points of the return map, $\mathbf{q}^* = \mathbf{f}^n(\mathbf{q}^*)$. Periodic motions require no energy loss at collisions since there are no energy storage or input mechanisms (e. g., springs or gravity) in the system to replenish energy losses.

For $H^*_{/P} = 0$, we get period-1 motions: constant-speed straight-line solutions ($E^* = \frac{1}{2}(V^*)^2 = E_0 \equiv$ const) where, as for the smooth skate, the energy is entirely translational.

For zero moment of inertia ($\rho = 0$) and a point mass located behind the front of the slot along the fore-aft axis of symmetry, period-2 motions can exist for any $E^* \neq 0$ and $H^*_{/P} \neq 0$. This case of zero moment of inertia is non-physical in the sense that we consider the motions of a massless structure. Nevertheless, we include it for curiosity's sake: see Appendix B.3 and Figure 10.

In addition to the fixed points of the return map, an equilibrium solution exists *without* collisions if the mass center lies within the slot ($-\Delta < L_0 < 0$): the skate can spin about the peg with constant angular rate when mass center and peg coincide. This solution has $\dot{V}_{eq} = 0$, $V_{eq} = 0$, and $\Omega_{eq} = \text{const}$, implying that $D_{eq} = -L_0$. For $D_{eq} = -L_0$ and $V(D_{eq}) = 0$, Equation (B.1) and Equations (3.3)–(3.4) give that the post-collision energy/momentum ratio necessary to achieve this spinning solution is

$$\frac{2\,{}^{i}E^+}{({}^{i}H^+_{/P})^2} = 1 \,. \tag{3.8}$$

3.1.2. Stability of Periodic Motions

We carry out a linearized stability analysis. Stability of the fixed point $\mathbf{q}^*$ is determined by the eigenvalues σ_j of the Jacobian of the return map evaluated at $\mathbf{q}^*$: $\mathbf{J} \equiv D\mathbf{f}(\mathbf{q}^*)$. Fixed points are asymptotically stable if all $|\sigma_j| < 1$. Due to conserved quantities and rotation and translation invariance, some of the eigenvalues are necessarily unity in our case. We consequently adopt the definition of stability used by Coleman, *et al.* [4]:

> The fixed point $\mathbf{q}^* \in \Sigma$ is *stable* if, for any $\epsilon > 0$, there exists $\delta > 0$ such that whenever $|\mathbf{q}_0 - \mathbf{q}^*| < \delta$, $|\mathbf{q}_n - \mathbf{q}^*| < \epsilon$ for all positive n. It is *asymptotically stable* if there exists $\delta > 0$ such that whenever $|\mathbf{q}_0 - \mathbf{q}^*| < \delta$, $|\mathbf{q}_n - \mathbf{q}^*| < \epsilon$ for all positive n and $\lim_{n\to\infty} \mathbf{q}_n = \mathbf{y}$ exists. Note that we do *not* insist that $\mathbf{y} = \mathbf{q}^*$, only that $|\mathbf{y} - \mathbf{q}^*| < \epsilon$; *therefore, our use of the term asymptotic stability is less restrictive than usual.* Clearly, if $\mathbf{y}$ exists, it must be a fixed point. Thus, we call a periodic motion asymptotically stable if, when slightly

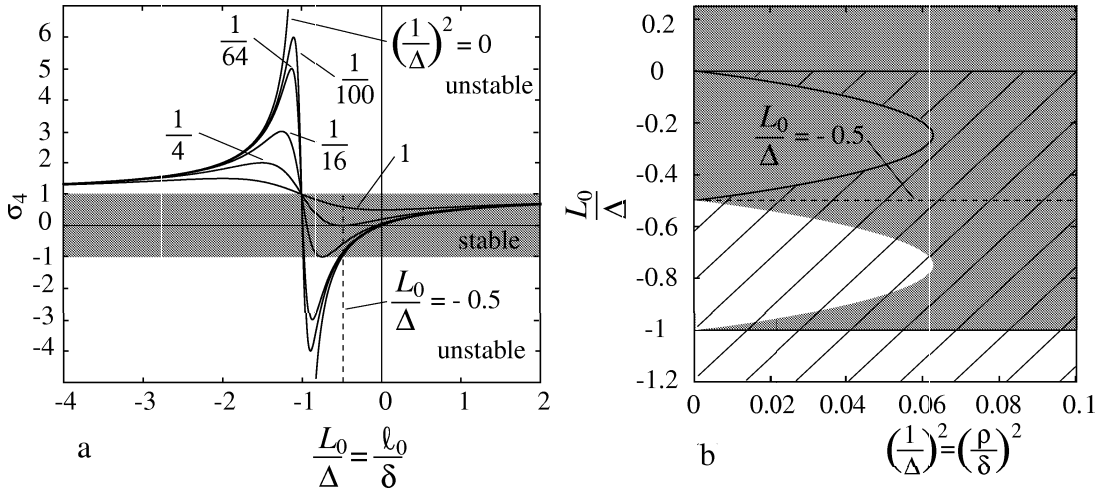

Fig. 2. (a) The analytically computed eigenvalue σ_4 of the Jacobian evaluated at the limit cycle fixed point for $V^* > 0$ is shown for $\frac{L_0}{\Delta}$ from -4 to 2 and for several values of $\left(\frac{1}{\Delta}\right)^2$ between 0 and 1. (b) The dependence of stability on Δ and L_0 for $V^* > 0$ and $V^* < 0$. The gray region indicates stability for $V^* > 0$ and the hashed region for $V^* < 0$; steady motions are unstable for parameters outside those regions. Note the region in which both the $V^* > 0$ and $V^* < 0$ solutions are simultaneously stable.

disturbed from it, the state asymptotically converges to some 'nearby' periodic motion. This is the strongest type of stability possible when there is a family of periodic motions, since the perturbed point $\mathbf{q}_0$ could just as well be a perturbation of $\mathbf{y}$ as of $\mathbf{q}^*$.

Stability of Constant-Speed Straight-Line (Period-1) Motions

Since we have a two-parameter family of period-1 fixed points, two eigenvalues will always be exactly equal to one. If all *other* eigenvalues are smaller than one in magnitude, then the fixed point is asymptotically stable in the weak sense described above. We find the Jacobian by linearising $\mathbf{f}$ of (B.3) at the period-1 fixed points $\mathbf{q}^* = \{0, E^*, \theta^*, 0\}^T$:

$$\mathbf{J} \equiv D\mathbf{f}(\mathbf{q}^*) = \begin{pmatrix} 0 & 0 & 0 & 0 \\ 0 & 1 & 0 & 0 \\ 0 & \dfrac{\partial f_3}{\partial E} & 1 & \dfrac{\partial f_3}{\partial H_{/P}} \\ 0 & 0 & 0 & \dfrac{1 + L_0(L_0 + \Delta)}{1 + (L_0 + (\Delta - D^+))^2} \end{pmatrix}, \tag{3.9}$$

where $D^+ = 0$ for $V^* > 0$ and $D^+ = \Delta$ for $V^* < 0$. Although we do not have an explicit expression for the θ component f_3, we can still find all eigenvalues. The characteristic equation yields:

$$\begin{aligned} &\sigma_1 = 0\,, && \sigma_{2,3} = 1\,, \\ &\sigma_4 = \frac{1 + L_0(L_0 + \Delta)}{1 + (L_0 + \Delta)^2} \text{ for } V^* > 0\,, && \sigma_4 = \frac{1 + L_0(L_0 + \Delta)}{1 + L_0^2} \text{ for } V^* < 0\,. \end{aligned} \tag{3.10}$$

These have the following interpretations: (1) $\sigma_1 = 0$ reflects the fact that the initially perturbed point $\mathbf{q}_0$ might lie off the Poincaré section Σ, but the next iterate $\mathbf{q}_1$ lies exactly on Σ; (2) $\sigma_{2,3} = 1$ since our system has a two-parameter family of fixed points; and (3) $|\sigma_4|$ determines stability type. This latter we call the stability eigenvalue.

Period-1 Stability Criteria

The expressions for σ_4 in Equation (3.10) determine stability criteria in terms of L_0 and Δ. We consider both $V^* > 0$ and $V^* < 0$. (In fact the system has a "reflection symmetry" about the mass center: taking L_0 to $-(L_0+\Delta)$ and V to $-V$, so we could restrict to $V^* > 0$ without loss of generality.) Constant-speed $V^* > 0$ straight-line motions are asymptotically stable for:

$$\frac{L_0}{\Delta} > -1 \quad \text{and} \quad \left(\frac{1}{\Delta}\right)^2 > -\frac{1}{2}\left(1+2\frac{L_0}{\Delta}\right)\left(1+\frac{L_0}{\Delta}\right) > 0\,. \tag{3.11}$$

Constant-speed $V^* < 0$ straight-line motions are asymptotically stable for:

$$\frac{L_0}{\Delta} < 0 \text{ and } \left(\frac{1}{\Delta}\right)^2 > -\frac{1}{2}\frac{L_0}{\Delta}\left(1+2\frac{L_0}{\Delta}\right) > 0\,. \tag{3.12}$$

Figure 2(a) shows the dependence of σ_4 on the ratios of mass center location to slot length ($\frac{L_0}{\Delta}$) and of radius of gyration to slot length ($\frac{\rho}{\delta} = \frac{1}{\Delta}$); to avoid clutter in the plot, we only show the $V^* > 0$ case. Figure 2(b) shows stability regions in parameter space for both $V^* > 0$ and $V^* < 0$. Note that, if the mass center lies within the slot ($-\Delta < L_0 < 0$), open sets of parameters exist for which (3.11–3.12) are *both* satisfied and forward and backward motions are simultaneously asymptotically stable.

For the special case of zero moment of inertia ($\rho = 0$), as $\frac{L_0}{\Delta} \to -1$ from left or right, σ_4 approaches ∞ or $-\infty$, respectively, and the eigenvalues indicate that period-1 motions are asymptotically stable for $\frac{L_0}{\Delta} > -\frac{1}{2}$. But, we have the more restrictive condition that the existence of period-1 motions requires $L_0 > 0$ (so that the skate does not change direction between collisions). Here is an example of a system with no dissipation but exponential stability: at each collision, a gain in energy of translation along the slot is exactly balanced by a loss in energy of rotation about the peg, yet angular momentum eventually decreases to zero!

Period-2 Stability for $\rho = I = 0$

The period-2 motions are always just neutrally stable; i. e., the eigenvalues of $\mathbf{J}^2$ evaluated at the fixed point are ($\sigma_1 = 0$, $\sigma_{2,3,4} = 1$).

Stability of the Spinning Solution

Linearising the system of governing equations (3.1), we find that the spinning solution $\mathbf{q}_{eq} = \{-L_0, 0, \theta_0 + \Omega_{eq}\tau, \Omega_{eq}\}^T$ is always of unstable saddle type, having eigenvalues 0 and $\pm\Omega_{eq}$.

3.1.3. Basins of Attraction

For $I \neq 0$ almost all initial conditions are attracted to straight-line constant-speed motions: $\Omega = 0$ with either (1) $V^* > 0$ or (2) $V^* < 0$. For any slot length, Δ, and center-of-mass position, L_0, and given any initial energy/angular momentum ratio $\left(\frac{2\,{}^0E^+}{({}^0H^+_{/P})^2}\right)$, Equations (B.5–B.8) in Appendix B.2.1 allow explicit computation of **(1)** velocity reversal positions in the slot and the sequence(s) of collision numbers after which reversals occur, and **(2)** the collision number after which no further reversals occur and the skate has settled down to travel in one direction or the other. We have not calculated a general expression for that sequence here though it can be done in principle; it is straightforward for given parameters and initial conditions. In particular, Equation (B.5) allows one to specify the

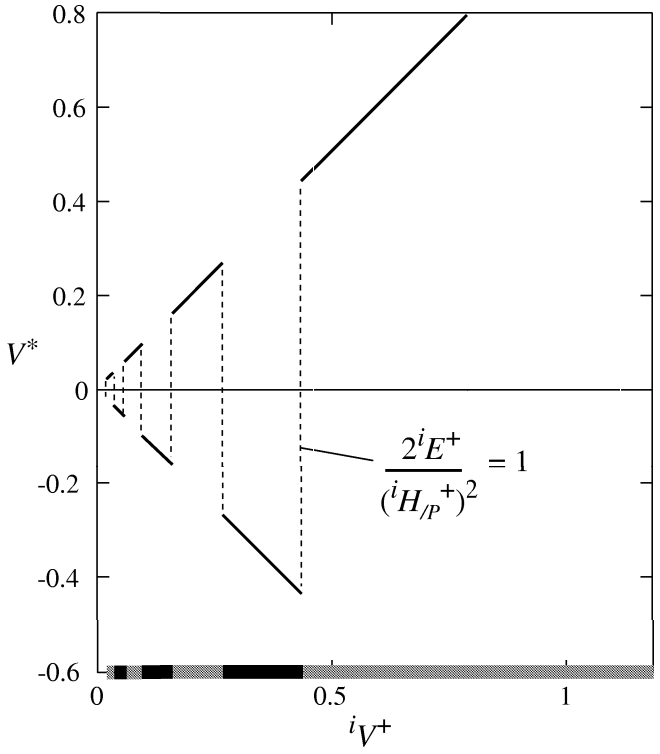

Fig. 3. Basins of attraction where $V^* > 0$ and $V^* < 0$ are simultaneously stable, for the special case $\frac{L_0}{\Delta} = -\frac{1}{2}$. Here, $L_0 = -\frac{1}{2}$, $\Delta = 1$, and ${}^iH^+_{/P} = 1$ (${}^i\Omega^+ = \frac{4}{5}$). The alternating open intervals attracted to either positive or negative solutions are shown on the horizontal axis: gray for $V^* > 0$ and black for $V^* < 0$. Vertical dashed lines indicate initial conditions attracted to spinning states. Only ${}^iV^+ > 0$ is shown, since the plot is symmetric about ${}^iV^+ = 0$. No reversals or spinning solutions occur for $\frac{2\,{}^{i+1}E^+}{({}^{i+1}H^+_{/P})^2} > 1$ (${}^iV^+ > 1/\sqrt{5}$, here).

energy/angular momentum ratio range that must be entered for a velocity reversal to be possible. Thus, for $L_0 > 0$, reversals can only occur if

$$\frac{1}{1+(L_0+\Delta)^2} < \frac{2\,{}^iE^+}{({}^iH^+_{/P})^2} < \frac{1}{1+L_0^2}\,; \tag{3.13}$$

and for $L_0 < -\Delta$:

$$\frac{1}{1+L_0^2} < \frac{2\,{}^iE^+}{({}^iH^+_{/P})^2} < \frac{1}{1+(L_0+\Delta)^2}\,. \tag{3.14}$$

However, the energy equation (3.3) supplies lower bounds for $\left(\frac{2^0E^+}{({}^0H^+_{/P})^2}\right)$ consistent with real velocities:

$$\frac{2\,{}^iE^+}{({}^iH^+_{/P})^2} > \frac{1}{1+L_0^2} \quad \text{for} \quad {}^iV^+ > 0;\ \frac{2\,{}^iE^+}{({}^iH^+_{/P})^2} > \frac{1}{1+(L_0+\Delta)^2} \quad \text{for} \quad {}^iV^+ < 0\,; \tag{3.15}$$

from this we conclude, for example, that if $L_0 > 0$ and $V > 0$ initially, no velocity reversal occurs. If $L_0 > 0$ and $V < 0$ initially, angular momentum increases on each collision and a single velocity

reversal occurs after the n'th collision drops $\left(\frac{2\,{}^{n}E^{+}}{({}^{n}H^{+}_{/P})^{2}}\right)$ into the range (3.13). Following this V remains positive and angular momentum decays to zero. Examples appear in Figures 4 and 5 below (the latter is actually for $L_0 < -\Delta < 0$ and $V > 0$ initially, but the symmetry noted in Section 3.1.2 implies that the behavior is similar if $L_0 > 0$ and $V < 0$ initially). For $-\Delta < L_0 < 0$ and $V > 0$ or $V < 0$, more complex behavior may occur, involving multiple reversals, and Equation (B.6) must be used with care, since it applies only to cases in which, after $\left(\frac{2\,{}^{n}E^{+}}{({}^{n}H^{+}_{/P})^{2}}\right)$ drops into the appropriate range, there is only one possible reversal point $D_c \in (0, \Delta)$. See Appendix B.2.1.

The two straight-line solutions $V^* > 0$ and $V^* < 0$ may be simultaneously stable, as noted in Section 3.1.2; the case shown in Figure 7 below provides an example. Given parameters for which both (3.11) and (3.12) hold, the basins of attraction for the two solutions are as follows:

1. For $\frac{2\,{}^{i}E^{+}}{({}^{i}H^{+}_{/P})^{2}} > 1$, no reversals occur and all initial states with ${}^{i}V^{+} > 0$ are attracted to solutions $V^* > 0$ and, likewise, all ${}^{i}V^{+} < 0$ are attracted to solutions $V^* < 0$.

2. For $0 < \frac{2\,{}^{i}E^{+}}{({}^{i}H^{+}_{/P})^{2}} < 1$, initial states ${}^{i}V^{+}$ of both signs can be attracted to either $V^* > 0$ or $V^* < 0$. For each ${}^{i}V^{+}$, the initial states fall into an alternating infinite sequence of open intervals in energy/momentum ratio: after one or more reversals, initial states in a given interval are attracted to, say, $V^* > 0$ solutions, those in the adjacent intervals are attracted to $V^* < 0$, etc. The boundaries of the intervals correspond to solutions that, after one or more collisions *and* reversals, are attracted to the unstable spinning equilibrium; that is, each initial state in the sequence eventually maps to one in which $\frac{2\,{}^{i}E^{+}}{({}^{i}H^{+}_{/P})^{2}} \equiv 1$, after which no further collisions occur, the mass center converges to the peg, and the skate spins indefinitely about it. As $\frac{2\,{}^{i}E^{+}}{({}^{i}H^{+}_{/P})^{2}} \to 0$, the width of these intervals decreases. We have not calculated the sequence in general although it can be done from Equations (B.3) and (B.4) for given parameters and initial conditions (the difficulty, as above, is that multiple reversals may occur).

We illustrate this in Figure 3 for the symmetric case of mass center at midpoint of the slot $\left(\frac{L_0}{\Delta} = -\frac{1}{2}\right)$, for which calculations simplify and the sequence of energy/momentum ratios leading to spinning can easily be found via a return map for energy/angular momentum ratio, derived from (B.3–B.4). Details are given in Section B.2.2. Similar results hold for different initial angular velocities.

Two Dissipative Systems with Analogous Behavior

The dynamical behavior of the discrete skate is analogous to two other dissipative systems [18]: (I) the classical driven pendulum with damping proportional to speed and constant applied torque [1] and (II) a rigid rimless spoked wheel confined to rolling up- or downhill in a vertical plane where energy is dissipated due to the spokes making perfectly plastic collisions with the ground [4, 5]. Depending on parameters, both these systems can possess distinct, coexisting, asymptotically stable states whose basins of attraction are separated by the (generalised) stable manifolds of unstable saddle-type solutions.

For the pendulum, the parameter is the torque/damping ratio and a saddle separatrix divides the basins of an 'overturning' solution (in which the work done by torque per revolution is balanced by damping), and a stable rest state. For the wheel (fixing inertia and spoke number), the parameter is the slope on which it rolls, and states leading to the wheel balancing on one spoke separate those

leading to downhill rolling with constant angular rate at each collision (gravity supplying the energy lost in collisions), from those leading to rocking back and forth on two spokes and eventually coming to rest on them after an *infinite* number of collisions in *finite* time.

4. Comparing Smooth and Discrete Skates

To compare the stability of the discrete to the smooth skate, we examine: (1) their stability eigenvalues in the limit as the slot length goes to zero and (2) the stability and instability modes available to each. First, we show typical phase space trajectories in arc length, energy, angular momentum coordinates for both systems in Figure 4 (centers of mass in front of the contact point and slot) and Figure 5 (centers of mass behind the contact point and slot). In both cases, the skates start with positive initial velocity $V_0 > 0$. In Figure 5, both skates reverse direction as their angular momenta pass through maxima.

4.1. Stability Eigenvalues

To compare the stability of the smooth and discrete systems, we expand the natural log of the discrete stability eigenvalue (σ_4) in a Taylor series, divide the result by the characteristic time τ^* between collisions in steady motion, and take the limit $\Delta \to 0$ (in nondimensional terms, $\tau^* = \frac{\Delta}{V^*}$). We obtain:

$$\xi_4 = \frac{V^*}{\Delta} \log\left(\frac{1 + L_0(L_0+\Delta)}{1+(L_0+\Delta)^2}\right) = V^*\left[-\frac{L_0}{1+L_0^2} + \frac{1}{2}\frac{L_0^2-2}{\left(1+L_0^2\right)^2}\Delta - \frac{1}{3}\frac{L_0\left(L_0^2-2\right)}{\left(1+L_0^2\right)^3}\Delta^2 + O(\Delta^3)\right]. \tag{4.1}$$

As $\Delta \to 0$, $\xi_4 \to -\frac{L_0 V^*}{1+L_0^2}$, in agreement with ξ_4 as calculated for the smooth skate in Section 2.1. This confirms the finding of Ruina [17] that the discrete skate inherits the asymptotic stability eigenvalues of the smooth skate even as dissipation goes to zero.

4.2. Stability and Instability Modes

While only one stability and one instability mode are available to the smooth skate, two stability and two instability modes are possible for the discrete skate. The discrete skate has a stability and instability mode like those of the smooth skate plus an additional stable and unstable mode. We show numerically generated plots of each mode in Figures 6–9. They may be summarized as follows:

- **Stability:**

  1. For $L > 0$ in the smooth skate (center of mass in front of the skate contact) and for $\frac{L_0}{\Delta} > -\frac{1}{2}$ in the discrete skate (center of mass in front of the center of the slot), a small angular velocity disturbance decays exponentially to zero and each system heads *smoothly* off in a slightly different heading (on the order of the disturbance) at a speed higher by a tiny amount (several orders of magnitude smaller than the disturbance.) See Figure 6.
  2. For $-1 < \frac{L_0}{\Delta} < -\frac{1}{2}$ and $\left(\frac{1}{\Delta}\right)^2 > -\frac{1}{2}\left(1+2\frac{L_0}{\Delta}\right)\left(1+\frac{L_0}{\Delta}\right) > 0$ in the discrete skate (mass center between the center and tail end of the slot), the system "wobbles" with exponentially decaying oscillations as it approaches a slightly different heading and slightly lower speed. This motion is not available to the smooth skate. See Figure 7.

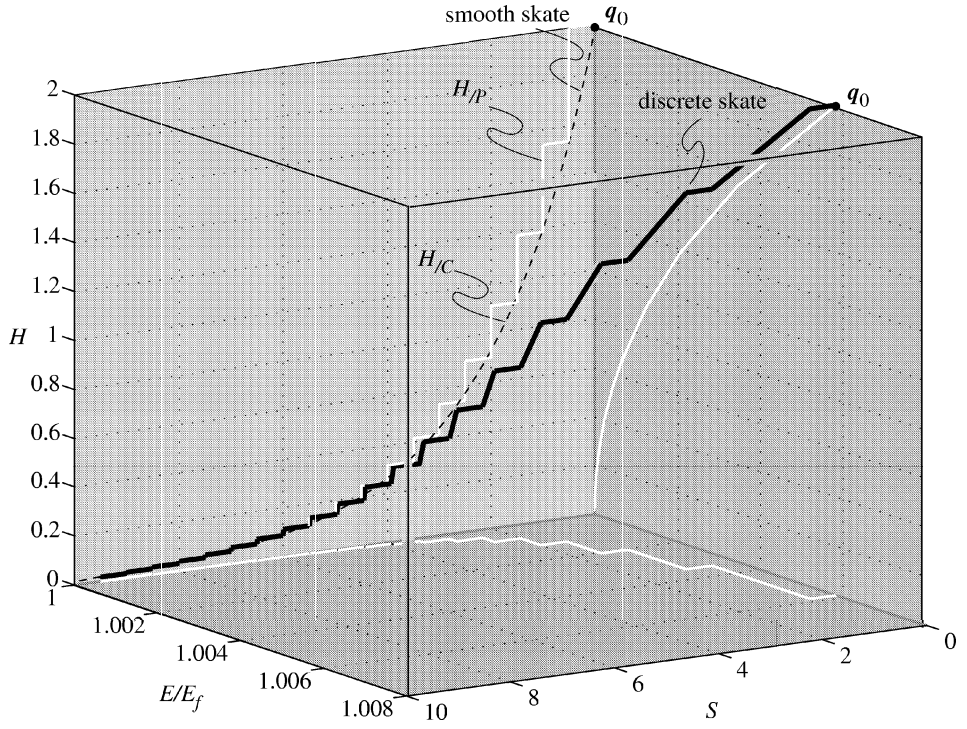

Fig. 4. For the smooth skate, the center of mass is in front of the skate contact point ($L = 1$) and for the discrete skate, in front of the slot ($L_0 = 1$). The slot length is $\Delta = \frac{1}{3}$. The plot shows very similar trajectories for the smooth and discrete skates even for a relatively large ratio of slot length to center of mass position. Energy is normalized with respect to the "final" energy, E_f (see Appendix B), so that all smooth skates start and end with unit energy and all discrete skates end with unit energy. Since energy is conserved globally for the smooth skate, its orbits lie on a constant energy plane. Both the smooth and discrete skates are given the same initial angular momentum and start with positive initial velocity $V_0 > 0$. The projections of the discrete skate trajectory are shown in white on each coordinate plane. The discrete skate trajectory is shown for 20 collisions. The discontinuities in the graphs of angular rates are due to the collisions. Note that angular momentum and energy are conserved between collisions for the discrete skate.

- **Instability:**

  1. For $L < 0$ in the smooth skate (center of mass behind the skate contact point) and for $\frac{L_0}{\Delta} < -1$ in the discrete skate (center of mass behind the tail end of slot), a small positive angular velocity disturbance at first grows exponentially. But, as the heading approaches near 90°, the smooth skate suddenly reverses direction (change of sign in velocity along the slot), continues to rotate (asymptotically approaching a final heading near 180° while the velocity along the slot asymptotically approaches near to the negative of its initial value and angular speed decays exponentially to zero. Like an unstable caster wheel, the smooth skate follows a cusp-like path on the plane, eventually reversing velocity and heading backwards close to its initial direction. See Figure 8.

     For the discrete skate, again, a small positive angular velocity disturbance at first grows exponentially. However, it suddenly reverses direction along the slot in its motion but at some *positive* angle that depends on Δ. The closer the slot length is to zero, the more the discrete skate behaves like the smooth skate.

     The final steady motions for the smooth or discrete skate, though not near the initial states, are again stable straight line motions.

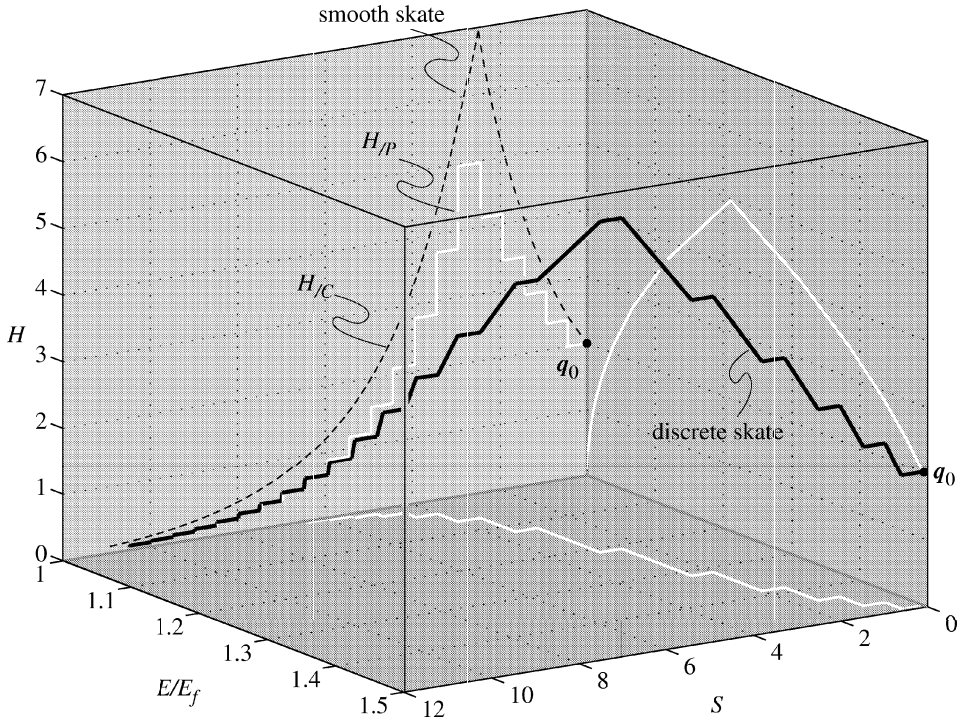

Fig. 5. For the smooth skate, the center of mass is behind the skate contact point ($L = -1$) and for the discrete skate, behind its slot ($L_0 = -1$). The slot length is $\Delta = \frac{1}{3}$. Again the plot shows similar trajectories for the smooth and discrete skates, even for a relatively large ratio of slot length to position of center of mass. Both the smooth and discrete skates are given the same initial angular momentum and start with positive initial velocity $V_0 > 0$. The projections of the discrete skate trajectory are shown on each coordinate plane. The discrete skate trajectory is shown for 22 collisions.

2. For $-1 < \dfrac{L_0}{\Delta} < -\dfrac{1}{2}$ and $\left(\dfrac{1}{\Delta}\right)^2 < -\dfrac{1}{2}\left(1+2\dfrac{L_0}{\Delta}\right)\left(1+\dfrac{L_0}{\Delta}\right)$ (center of mass between the center and tail end of the slot), the skate at first wobbles with exponentially growing oscillations about its initial direction, suddenly reverses direction at some positive or negative angle, and then asymptotically wobbles to some final positive or negative angle. The transitional and final angles are highly sensitive to the parameters. In addition, the skate speeds and slows between each collision: a "lurching" type of motion. See Figure 9. This type of behavior is not available to the smooth skate.

Finally, Figure 10 illustrates the neutrally stable period-2 motions obtained for $\rho = I = 0$, as noted at the end of Section 3.1.2.

5. Conclusions

In this paper, we have extended the analysis of the discrete Chaplygin sleigh or skate presented in Ruina [17]. We have developed explicit Poincaré mappings describing motions of the system in terms of energy and angular momentum, and used these to calculate the discrete skate's linear stability eigenvalue and hence provide explicit stability boundaries in parameter space. We show that the stability eigenvalue approaches that of the smooth skate in the limit as the slot length goes to zero. Furthermore, the discrete skate has somewhat broader stability ranges than its smooth sister, in terms of mass center position, and it exhibits a greater variety of behaviors, including growing and decaying

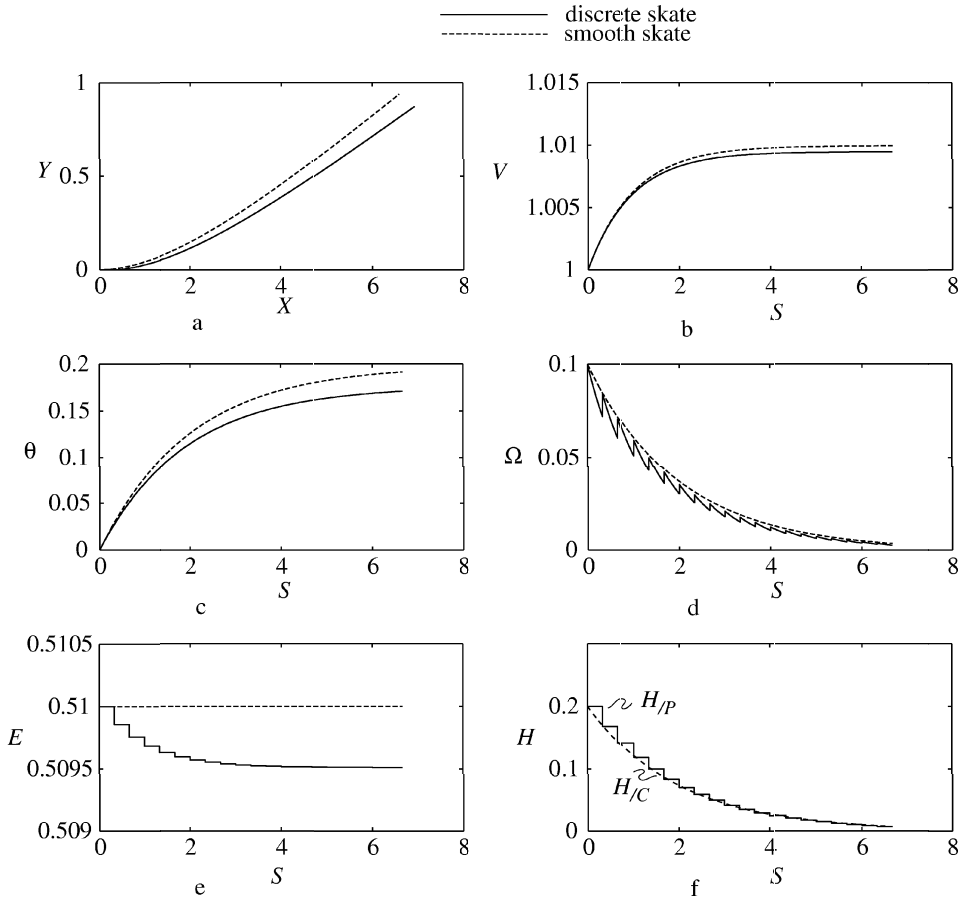

Fig. 6. For the smooth skate, the center of mass is in front of the skate contact point ($L = 1$) and for the discrete skate, in front of its slot ($L_0 = 1$). The slot length is $\Delta = \frac{1}{3}$. In this and subsequent figures, the solid lines are for the discrete skate and the dashed lines are for the smooth skate; also, $H_{/C}$ is the angular momentum about the smooth skate contact point and $H_{/P}$ is the angular momentum about a peg for the discrete skate. The plots show similar *stable trajectories* for the smooth and discrete skates. In this and subsequent figures, (a) shows the paths of the smooth skate contact point and the front of the discrete skate slot. The discrete skate plots are shown for 20 collisions. The discontinuities in the plots for the discrete skate are due to the collisions. Note that in (e) and (f) of this and subsequent figures, energy and angular momentum are conserved between collisions.

oscillations in angular momentum and velocity, orbits with multiple reversals, and coexistence of stable straight-line motions in both forward and reverse directions.

Acknowledgments

The authors thank Andy Ruina for suggesting Figures 4 and 5; pointing out the velocity scaling and the analogy of the skate to the forced, damped pendulum and the 2D rimless wheel; showing how to compare the eigenvalues of the discrete and smooth skates; and his editing of this paper. PH was partially supported by DoE: DE–FG02–95ER25238 and DARPA/ONR: N00014–98–1–0747.

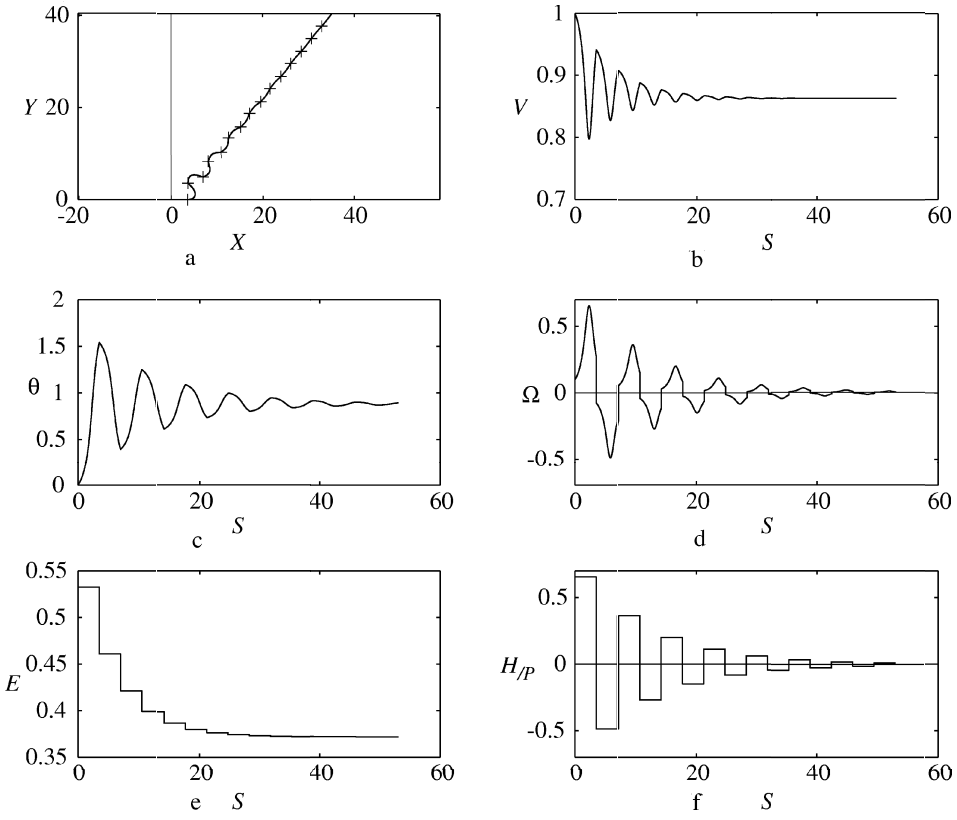

Fig. 7. The center of mass is between the rear end and center of the slot $\left(\frac{L_0}{\Delta} = -\frac{2}{3}\right)$ and $\left(\frac{1}{\Delta}\right)^2 = \left(\frac{\rho}{\delta}\right)^2 = 0.08$. The plots show *stable* behavior for the discrete skate not available to the smooth skate – the system "wobbles" with exponentially decaying oscillations as it approaches a slightly different heading and slightly lower speed. In Figure (a) and subsequent figures, the peg locations are marked with plus ("+") signs. The plots are shown for 15 collisions.

A. Smooth Skate Closed Form Solutions

To find closed form solutions for state variables as a function of arc length S, we must take into account that, when the skate goes unstable for $L < 0$, the velocity of point C changes sign at a particular point along the skate path. S_c is the arc length at the change in sign of velocity for $L < 0$:

$$S_c = S_0 - \frac{1+L^2}{2L} \ln\left(1 + \frac{V_0^2}{\Omega_0^2(1+L^2)}\right). \tag{A.1}$$

So, for $S > S_c$, $V < 0$. The closed form solutions may now be written:

$$\begin{aligned}
V(S) &= K\sqrt{V_0^2 + \Omega_0^2\,(1+L^2))\left(1 - e^{-K\frac{2L}{1+L^2}(S-S_0)}\right)}, \\
\theta(S) &= \theta_0 + K\frac{\sqrt{1+L^2}}{L}\left[\sin^{-1}\left(\frac{1}{\sqrt{\frac{V_0^2}{\Omega_0^2(1+L^2)}+1}}\right) - \sin^{-1}\left(\frac{e^{-K\frac{L}{1+L^2}(S-S_0)}}{\sqrt{\frac{V_0^2}{\Omega_0^2(1+L^2)}+1}}\right)\right], \quad \text{and} \\
\Omega(S) &= \Omega_0\, e^{-K\frac{L}{1+L^2}(S-S_0)},
\end{aligned} \tag{A.2}$$

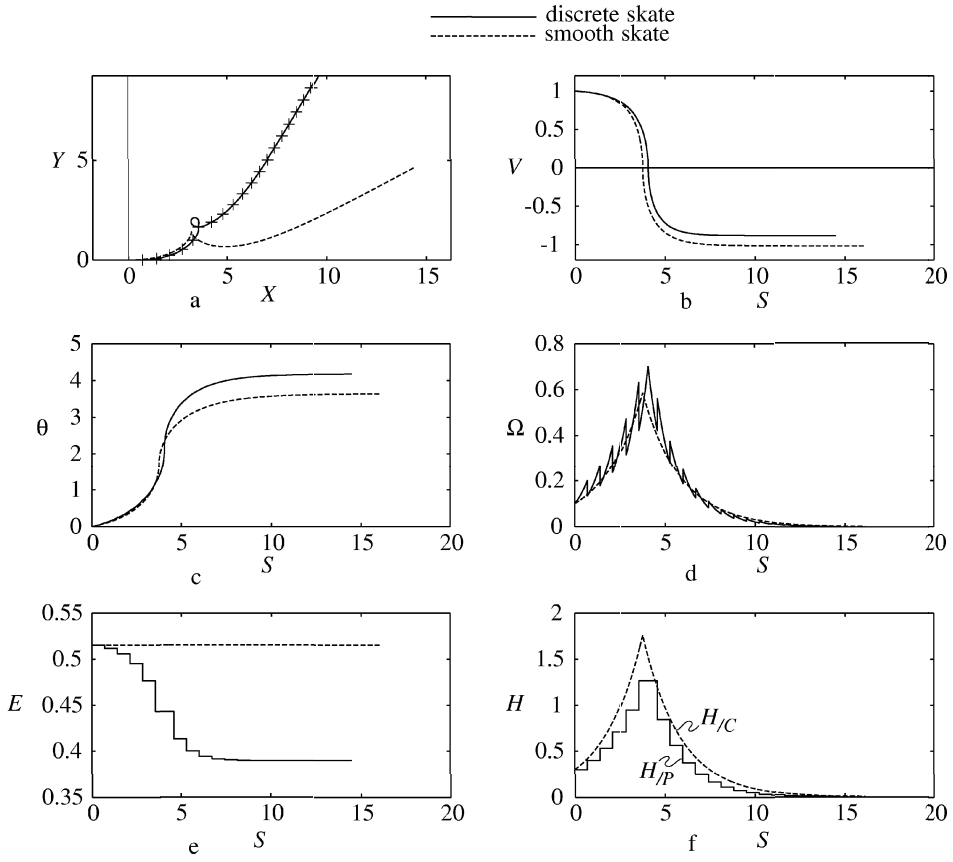

Fig. 8. For the smooth skate, the center of mass is behind the skate contact point ($L = -\sqrt{2}$) and for the discrete skate, behind the tail end of its slot ($L_0 = -\sqrt{2}$). The slot length is $\Delta = \dfrac{\sqrt{2}}{2}$. The plots show similar *initially unstable* orbits for the smooth and discrete skates. The discrete skate plots are shown for 18 collisions.

where for $V_0 > 0$, K is defined as

$$K = \begin{cases} 1 & S > S_0 \quad \text{and} \quad L > 0 \quad \textit{or} \quad S < S_c \quad \text{and} \quad L < 0\,, \\ -1 & S > S_c \quad \text{and} \quad L < 0\,. \end{cases} \,. \tag{A.3}$$

Energy–Momentum Formulation

Recasting the problem in terms of energy and momentum as functions of arc length S, the state of the system can be characterized by the nondimensional quantities:

$$E(S) = \frac{1}{2}\left[V^2(S) + (1+L^2)\Omega^2(S)\right] = E_0 = \text{const}\,,$$

$$\theta(S) = \theta_0 + K\frac{\sqrt{1+L^2}}{L}\left[\sin^{-1}\left(\frac{1}{\sqrt{2\dfrac{E_0(1+L^2)}{(H^0_{/C})^2}}}\right) - \sin^{-1}\left(\frac{e^{-K\frac{L}{1+L^2}(S-S_0)}}{\sqrt{2\dfrac{E_0(1+L^2)}{(H^0_{/C})^2}}}\right)\right], \quad \text{and} \tag{A.4}$$

$$H_{/C}(S) = (1+L^2)\Omega(S) = H^0_{/C}\; e^{-K\frac{L}{1+L^2}(S-S_0)}\,.$$

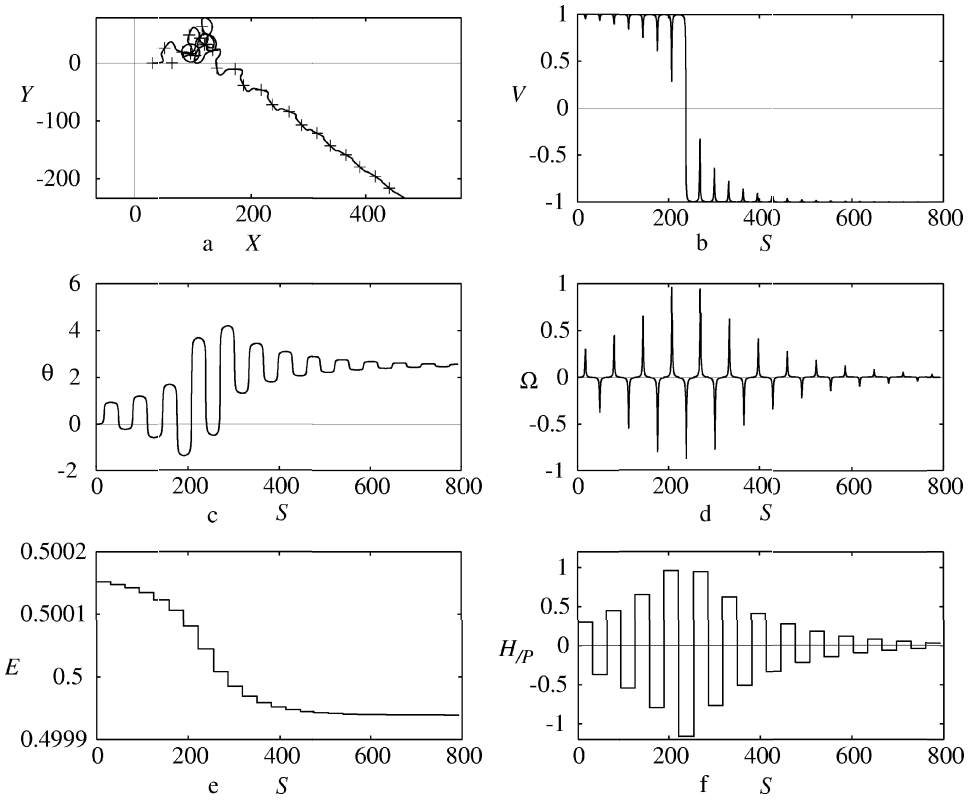

Fig. 9. The center of mass is between the rear end and center of the slot $\left(\frac{L_0}{\Delta} = -0.55\right)$ and $\left(\frac{1}{\Delta}\right)^2 = \left(\frac{\rho}{\delta}\right)^2 = 0.001$. The plots show *unstable* behavior for the discrete skate not available to the smooth skate — the system "wobbles" with exponentially increasing oscillations until it reverses direction, eventually approaching some final angle and a speed along the slot nearly equal to its initial value. The plots are shown for 25 collisions.

The state vector is now $\mathbf{q} = \{S, E, \theta, H_{/C}\}^T$. Equilibrium straight-line solutions are

$$H^*_{/C} = 0 \quad \text{and} \quad E^* = \frac{1}{2}(V^*)^2, \tag{A.5}$$

where the energy is all in translation. In terms of energy and momentum, the change in sign of the velocity of the contact point occurs at:

$$S_c = S_0 - \frac{1+L^2}{2L} \ln\left(2\frac{E_0(1+L^2)}{(H^0_{/C})^2}\right). \tag{A.6}$$

B. Discrete Skate Formulation

We summarize here solution of the governing equations of motion, derivation of the return map and calculation of fixed points and their stability.

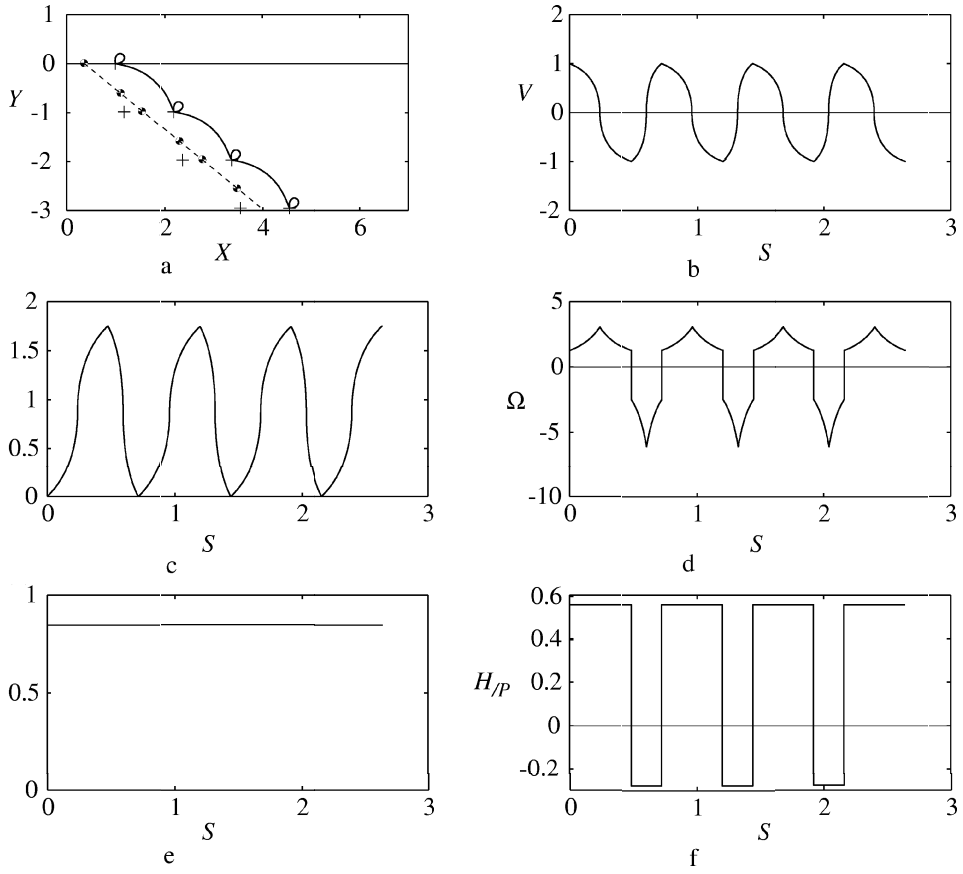

Fig. 10. A point mass is located between the rear end and center of the slot $\left(\frac{L_0}{\Delta} = -\frac{2}{3}\right)$ and the moment of inertia of the skate is zero ($\rho = 0$). The plots show period-2 behavior for the discrete skate not available to the smooth skate. Note in (a) that the center of mass travels along a straight line; its position is shown just after each collision. Note in (e) that no energy is lost at collisions.

B.1. Solution of Equations of Motion between Collisions

Closed form solutions of (3.1) for V and Ω can be found as functions of D (the position of the peg along the slot) between collisions:

$$[V(D)]^2 = V_0^2 + \frac{(D - D_0)(2L_0 + D + D_0)(1 + (L_0 + D_0)^2)}{1 + (L_0 + D)^2}\Omega_0^2 \quad \text{and}$$
$$\Omega(D) = \Omega_0 \frac{1 + (L_0 + D_0)^2}{1 + (L_0 + D)^2}\,; \tag{B.1}$$

the latter is just conservation of angular momentum about the peg. Using this, conservation of energy, and observing from the governing equations (3.1) that $\frac{d\theta}{dD} = \frac{\Omega}{V}$, the angle θ between collisions can be expressed as an elliptic integral

$$\theta(D) = \theta_0 + \int_{D_0}^{D} \frac{dD'}{\sqrt{\frac{1 + (L_0 + D')^2}{1 + (L_0 + D_0)^2}\left[\left(\frac{V_0}{\Omega_0}\right)^2 \frac{1 + (L_0 + D')^2}{1 + (L_0 + D_0)^2} + (D' - D_0)(2L_0 + D' + D_0)\right]}}\,, \tag{B.2}$$

where the prime ($'$) indicates a dummy integration variable.

B.2. Return map

The return map is derived by composition of the collision rule (3.7) in terms of energy and angular momentum, with the solutions (B.1-B.2) of the governing equations between collisions, and using conservation of energy and angular momentum about the peg between collisions. There are two cases: **(1)** the sign of velocity along the slot just after a collision is the same as its sign just before the next collisions and **(2)** the velocity along the slot changes sign in between collisions.

1. $\mathrm{sgn}[({}^{i+1}V^-)({}^iV^+)] = 1$

$$
\begin{aligned}
{}^{i+1}D^+ &= {}^i D^+ ,\\
{}^{i+1}E^+ &= {}^iE^+ + {}^iC_1^+ \left({}^iH_{/P}^+\right)^2 ,\\
{}^{i+1}\theta^+ &= {}^i\theta^+ ,\\
&\quad + \int_{{}^iD^+}^{\Delta-{}^iD^+} \frac{dD'}{\sqrt{(1+(L_0+D')^2)\left[2\dfrac{{}^iE^+\left(1+(L_0+D')^2\right)}{({}^iH_{/P}^+)^2}-1\right]}} \equiv {}^i\theta^+ + f_3({}^iE^+, {}^iH_{/P}^+) ,\\
{}^{i+1}H_{/P}^+ &= {}^iC_2^+\,{}^iH_{/P}^+ ,\\
{}^iC_1^+ &= -\frac{1}{2}\frac{\Delta^2}{\left[1+(L_0+(\Delta-{}^iD^+))^2\right]^2\left[1+(L_0+{}^iD^+)^2\right]} , \quad \text{and}\\
{}^iC_2^+ &= \frac{1+L_0(L_0+\Delta)}{1+(L_0+(\Delta-{}^iD^+))^2} .
\end{aligned}
\tag{B.3}
$$

2. $\mathrm{sgn}[({}^{i+1}V^-)({}^iV^+)] = -1$

$$
\begin{aligned}
{}^{i+1}D^+ &= \Delta - {}^iD^+ ,\\
{}^{i+1}E^+ &= {}^iE^+ + {}^iC_1^+ \left({}^iH_{/P}^+\right)^2 ,\\
{}^{i+1}\theta^+ &= {}^i\theta^+ + 2\int_{{}^iD^+}^{D_c} \frac{dD'}{\sqrt{(1+(L_0+D')^2)\left[2\dfrac{{}^iE^+\left(1+(L_0+D')^2\right)}{({}^iH_{/P}^+)^2}-1\right]}} ,\\
{}^{i+1}H_{/P}^+ &= {}^iC_2^+\,{}^iH_{/P}^+ ,\\
{}^iC_1^+ &= -\frac{1}{2}\frac{\Delta^2}{\left[1+(L_0+{}^iD^+)^2\right]^2\left[1+(L_0+(\Delta-{}^iD^+))^2\right]} , \quad \text{and}\\
{}^iC_2^+ &= \frac{1+L_0(L_0+\Delta)}{1+(L_0+{}^iD^+)^2} .
\end{aligned}
\tag{B.4}
$$

Here ${}^iD^+ = 0$ for ${}^iV^+ > 0$ and ${}^iD^+ = \Delta$ for ${}^iV^+ < 0$. Note the changes in ${}^iC_1^+$ and ${}^iC_2^+$ between cases (1)–(2).

B.2.1. Velocity Reversals

The point(s) D_c along the slot where $V(D_c) = 0$ and the skate reverses direction between collisions may be found from the conservation laws (3.3–3.4) as the relevant solution(s) $D_c \in (0, \Delta)$ of:

$$D_c = -L_0 \pm \sqrt{\left[\frac{({}^iH^+_{/P})^2}{2\,{}^iE^+} - 1\right]}. \tag{B.5}$$

Clearly, for $L_0 > 0$ (resp. $L_0 < -\Delta$), only the positive (resp. negative) solutions are relevant, but *both* solutions may lie within the slot for $-\Delta < L_0 < 0$. However, relevant solutions occur only when the "energy/angular momentum" ratio $\left(\frac{2\,{}^iE^+}{({}^iH^+_{/P})^2}\right)$ falls into an appropriate range. Given the ratio at step i, one can compute the number of additional iterates necessary for this to occur from the conservation laws and the mapping rule (B.3), by seeking a sign change in the quantity $V(D)$, thus obtaining:

$$n = \left\lfloor \frac{\log\left[1 + \frac{(1 - ({}^iC_2^+)^2)}{{}^iC_3^+}\left(\frac{2\,{}^iE^+}{({}^iH^+_{/P})^2}\left(1 + (L_0 + {}^iD^+)^2\right) - 1\right)\right]}{\log\left[({}^iC_2^+)^2\right]} \right\rfloor, \tag{B.6}$$

where

$${}^iC_3^+ = \frac{\mathrm{sgn}[{}^iV^+]\Delta(2L_0 + \Delta)}{1 + (L_0 + (\Delta - {}^iD^+))^2}. \tag{B.7}$$

(The "$\lfloor x \rfloor$" notation has the usual meaning of the greatest integer less than or equal to a number x.) Note that Equation (B.6) applies *only* in cases in which there is at most a single turning point $D_c \in (0, \Delta)$: i.e., to *all* $L_0 > 0$ and $L_0 < -\Delta$, but only to *some* subcases of $-\Delta < L_0 < 0$. Specifically, if

$$\min\left\{\frac{1}{1 + L_0^2}, \frac{1}{1 + (L_0 + \Delta)^2}\right\} < \frac{2\,{}^iE^+}{({}^iH^+_{/P})^2} < 1, \tag{B.8}$$

then (B.5) has two relevant solutions, reversals can occur for both ${}^iV^+ > 0$ and ${}^iV^+ < 0$, and (B.6) does not predict n. One can compute the number of steps needed to achieve (B.8) from given initial data, but we have not been able to find a "simple" expression analogous to (B.6).

B.2.2. Energy Analysis

Let ${}^iE^+$ be the energy of the skate after which no more reversals can occur. Then, its total energy n collisions after the i'th is given by the geometric series:

$$\begin{aligned} {}^{i+n}E^+ &= {}^iE^+ + {}^iC_1^+({}^iH^+_{/P})^2 \sum_{j=0}^{n} ({}^iC_2^+)^{2j} \\ &= {}^iE^+ + {}^iC_1^+ \frac{1 - ({}^iC_2^+)^{2n}}{1 - ({}^iC_2^+)^2}({}^iH^+_{/P})^2 \quad \text{(summing the series for finite } n\text{)}. \end{aligned} \tag{B.9}$$

We find the final energy in terms of that after the $i_{\rm th}$ collision as $n \to \infty$ to be:

$$\begin{aligned} E_f &= {}^iE^+ + \lim_{n\to\infty} {}^iC_1^+ \frac{1-({}^iC_2^+)^{2n}}{1-({}^iC_2^+)^2} ({}^iH_{/P}^+)^2 \\ &= {}^iE^+ + \frac{{}^iC_1^+}{1-({}^iC_2^+)^2} ({}^iH_{/P}^+)^2 \,, \end{aligned} \tag{B.10}$$

where convergence requires that $|{}^iC_2^+| < 1$ or

$$\begin{aligned} -\frac{L_0}{\Delta} + 2\frac{L_0}{\Delta}\left(1-\frac{{}^iD^+}{\Delta}\right) + \left(1-\frac{{}^iD^+}{\Delta}\right)^2 > 0 \quad \text{and} \\ \left(\frac{1}{\Delta}\right)^2 > -\frac{L_0}{\Delta}\left[\frac{L_0}{\Delta}+\frac{1}{2}+\left(1-\frac{{}^iD^+}{\Delta}\right)\right] - \frac{1}{2}\left(1-\frac{{}^iD^+}{\Delta}\right)^2 > 0 \,. \end{aligned} \tag{B.11}$$

These conditions are exactly those for asymptotic stability of period-1 fixed points (Equation(3.11)). We use Equation (B.10) to generate Figures 4–5.

We can rewrite Equation (B.10) in terms of initial and final velocities and angular rate to get, for $V_f > 0$:

$$V_f^2 = ({}^iV^+)^2 + (1+L_0^2)\left[1 - \frac{\Delta}{(L_0+\Delta)\,(2+(L_0+\Delta)(2L_0+\Delta))}\right]({}^i\Omega^+)^2 \,. \tag{B.12}$$

A similar expression can be obtained for $V_f < 0$.

Interestingly, for the special "symmetric" case of mass center located at the center of the slot ($\frac{L_0}{\Delta} = -\frac{1}{2}$), Equation (B.12) shows that the velocity along the slot after many collisions returns to its initial value, $V_f = V_0$ (the skate has no sense of whether it is going forwards or backwards). Also, for this case the sequence of energy/momentum ratios leading to the unstable spin state can easily be found via a return map for energy/angular momentum ratio, derived from (B.3–B.4), *cf.* Equation (B.9). From this we find a monotone decreasing sequence of energy/momentum ratios for which the n_{th} element of the sequence arrives at the state necessary to approach the spinning solution (following n collisions). This sequence may be rewritten in terms of velocity along the slot and angular rate as

$$\frac{({}^nV^+)^2}{({}^n\Omega^+)^2} = (1+L_0^2)^2\left(C_2^{2n} - 2C_1\frac{1-C_2^{2n}}{1-C_2^2}\right) - (1+L_0^2), \qquad n = 0,1,2,3,\ldots \tag{B.13}$$

(we may drop the pre- and post-superscripts from C_1 and C_2 since for the symmetric case $\frac{L_0}{\Delta} = -\frac{1}{2}$ their values coincide for $V > 0$ and $V < 0$). Using the fact (above) that $V^* = \pm {}^iV^+$, Equation (B.13) leads to the plot of basins of attraction for $V^* > 0$ and $V^* < 0$ shown in Figure 3.

B.3. Fixed Points

The return map (Equation(B.3)) shows that periodic motions with lossless collisions require that

$${}^iC_1^+ (H_{/P}^*)^2 = 0 \,. \tag{B.14}$$

This condition is satisfied if: **(1)** $H_{/P}^* = 0$ or **(2)** ${}^iC_1^+ = 0$.

1. For $H^*_{/P} = 0$, we get period-1 motions: constant-speed straight-line solutions ($E^* = \frac{1}{2}(V^*)^2 = E_0 \equiv$ constant) where, as for the smooth skate, the energy is all in translation. The *inter collision duration* is $\tau^* = \frac{\Delta}{V^*} = \frac{\Delta}{\sqrt{2E^*}}$. For fixed system parameters (L_0, Δ) there is a two-dimensional family of period-1 motions parameterized by speed V^* and heading θ^*.

2. For ${}^iC_1^+ = 0$, either **(a)** $\Delta = 0$ (slot length is zero) or **(b)** $\rho \to 0$ (radius of gyration goes to zero). Case (a) is the smooth skate. In case (b), the skate becomes a massless structure with a point mass located along its fore-aft axis of symmetry.

Special Limiting Case ($\lim \rho \to 0$): For $\rho = 0$, taking angular momentum balance about the mass center shows that no net moment can act on the skate structure. Since the constraint force ($F\hat{\mathbf{e}}_n$) is the only force acting on the skate, a vanishing applied moment requires that $F = 0$. Then, linear momentum balance implies that the acceleration of the center of mass is zero; hence, the mass center must travel in a straight line at constant velocity in the direction of the initial velocity vector throughout the skate's motion, which is therefore completely determined by geometry.

For ease of analysis, we first find the simplified return map for angular momentum with zero moment of inertia:

$$ {}^{i+1}H^+_{/P} = {}^iC_2^+ \, {}^iH^+_{/P} \,, \tag{B.15}$$

where now

$$ {}^iC_2^+ = \frac{L_0(L_0+1)}{(L_0 + (1 - {}^iD^+))^2} \,, \tag{B.16}$$

and, since $\rho = 0$, we have nondimensionalized with respect to the slot length δ:

$$ L_0 = \frac{\ell_0}{\delta} \,, \quad D = \frac{d}{\delta} \,, \quad V = \frac{v}{v_0} \,, \quad \Omega = \frac{\omega}{v_0}\delta \,, \quad \tau = \frac{tv_0}{\delta} \,, \quad \text{and } (\dot{}) = \frac{d(\quad)}{d\tau} \,, \tag{B.17}$$

so the nondimensional slot length is $\Delta = \frac{\delta}{\delta} = 1$. We can get period-1 solutions for ${}^iC_2^+ = 1$, which holds only for the trivial case $\delta = 0$. Thus, the only period-1 solutions in this case are again the constant-speed straight-line motions or $H^*_{/P} = 0$.

When $\rho = 0$ and given arbitrary initial conditions, the velocity along the slot will change sign once after each collision for $L_0 < 0$; i. e., according to Equation (B.6), $n = 0$. That the skate center-of-mass must travel in a straight line in the direction of the initial velocity vector corroborates this fact; if the center-of-mass is behind the slot and must travel in a straight line, the skate will "flip" around the current peg and reverse direction with respect to it. This periodic flip-flop in the sign of velocity along the slot raises the question of whether period-2 solutions exist.

Over two collisions, we have
${}^{i+2}H^+_{/P} = {}^{i+1}C_2^+ \, {}^iC_2^+ \, {}^iH^+_{/P}$. Period-2 solutions require ${}^{i+1}C_2^+ \, {}^iC_2^+ = 1$ *and* the flip-flop in velocity along the slot after each collision ($L_0 < 0$, $\frac{L_0}{\Delta} \neq -1$). (For $\frac{L_0}{\Delta} = -1$ and given arbitrary initial conditions, the skate stops translating after one collision and spins infinitely fast about a peg.) For $\rho = 0$, using (B.16) with ${}^iD^+ = 0$, ${}^{i+1}D^+ = \Delta = 1$ (or *vice versa*), we find

${}^iC_2^+ = \frac{L_0}{L_0+1} = \left({}^{i+1}C_2^+\right)^{-1}$; thus neutrally stable period-2 solutions exist, as shown in Figure 10.

No other periodic solutions exist. For ρ small but nonzero, however, numerical studies show that *quasi-periodic* motions exist closely resembling those in Figure 10; after many collisions and looping motions, the skate eventually settles into a straight-line motion.

References

[1] *A. A. Andronov, A. A. Vitt, S. E. Khaikin.* Theory of Oscillators. Dover, 1966.

[2] *A. M. Bloch.* Asymptotic Hamiltonian dynamics: the Toda lattice, the three-wave interaction and the nonholonomic Caplygin sleigh. Preprint, Dept of Mathematics, University of Michigan, 1999. unpublished.

[3] *M. Bühler, D. E. Koditschek.* From Stable to Chaotic Juggling: Theory, Simulation, and Experiments. 1990 IEEE International Conference on Robotics and Automation, IEEE Robotics and Automation Society, 1990, P. 1976–1981. The Proc. are from a conference held during May 13-18, 1990 in Cincinnati, Ohio.

[4] *M. Coleman, A. Chatterjee, A. Ruina.* Motions of a Rimless Spoked Wheel: A Simple 3D System with Impacts. Dynamics and Stability of Systems, 1997, V. 12, №. 3, P. 139–169.

[5] *M. J. Coleman.* A Stability Study of a Three-dimensional Passive-dynamic Model of Human Gait. Cornell University, 1998, Ithaca, NY.

[6] *M. J. Coleman, A. Ruina.* An uncontrolled walking toy that cannot stand still. Phys. Rev. Let., 1998, V. 80, № 16, P. 3658–3661.

[7] *M. Garcia, A. Chatterjee, A. Ruina, M. J. Coleman.* The Simplest Walking Model: Stability, Complexity, and Scaling. ASME J. Biomech. Eng., 1998, V. 120, № 2, P. 281–288.

[8] *J. Guckenheimer, P. Holmes.* Nonlinear Oscillations, Dynamical Systems, and Bifurcations of Vector Fields. Springer–Verlag, 1983, New York.

[9] *Y. Hurmuzlu.* Dynamics of Bipedal Gait: Part I — Objective functions and the contact event of planar five-link biped. J. of Applied Mechanics, 1993, V. 60, P. 331–337.

[10] *Y. Hurmuzlu.* Dynamics of Bipedal Gait: Part II — Stability analysis of a planar five-link biped. J. of Applied Mechanics, 1993, V. 60, P. 337–343.

[11] *T. McGeer.* Passive Dynamic Walking. Intern. J. Robot. Res., 1990, V. 9, № 2, P. 62–82.

[12] *T. McGeer.* Passive Walking with Knees. Proc., 1990 IEEE International Conference on Robotics and Automation, 1990, P. 1640–1645, IEEE, Los Alamitos, CA.

[13] *T. McGeer.* Passive Dynamic Biped Catalogue. Proc., Experimental Robotics II: The 2nd International Symposium. 1992, P. 465–490, Springer–Verlag, Berlin.

[14] *J. I. Neimark, N. A. Fufaev.* Dynamics of Nonholonomic Systems. AMS, 1972, V. 33, Translations of Mathematical Monographs, Providence, Rhode Island.

[15] *R. Pratap, S. Mukherjee, F. C. Moon.* Dynamic Behavior of a Bilinear Hysteretic Elasto-plastic Oscillator, Part I: Free Oscillations. J. of Sound and Vibration, 1994, V. 172, № 3, P. 321–337.

[16] *R. Pratap, S. Mukherjee, F. C. Moon.* Dynamic Behavior of a Bilinear Hysteretic Elasto-plastic Oscillator, Part II: Oscillations Under Periodic Impulse Forcing. J. of Sound and Vibration, 1994, V. 172, № 3, P. 339–358.

[17] *A. Ruina.* Nonholonomic Stability Aspects of Piecewise Holonomic Systems. Reports on Mathematical Physics, 1998, V. 42, № 1/2, P. 91–100.

[18] *A. Ruina.* Personal communication. 1999. unpublished.

[19] *J. Schmitt, P. Holmes.* Mechanical Models for insect Locomotion: Dynamics and stability in the horizontal Plane. 1999. Preprint, Department of Mechanical and Aerospace Engineering. Princeton University.

[20] *S. W. Shaw, P. J. Holmes.* A periodically Forced Piecewise Linear Oscillator. J. of Sound and Vibration, 1983, V. 90, № 1, P. 129–155.

[21] *S. W. Shaw, R. H. Rand.* The Transition to Chaos in a Simple Mechanical System. International Journal of Non-Linear Mechanics, 1989, V. 24, № 1, P. 41–56.